J Mater Sci (2024) 59:12812–12829

Thermal spray to embed optical fibers for the monitoring and protection of metallic structures

Daniela Rigamonti[1,*], Hector Reynaldo Meneses Costa[2], Gianmarco Bilotti[1], and Paolo Bettini[1]

[1] *Aerospace Science and Technology Department of Politecnico Di Milano, Milan, Italy*
[2] *Federal Centre for Technological Education Celso Suckow da Fonseca—CEFET/RJ, Rio de Janeiro, Brazil*

Received: 29 January 2024
Accepted: 14 June 2024
Published online: 4 July 2024

ABSTRACT

In the framework of using fiber optics (FO) for structural health monitoring, a true challenge is to fix the fiber onto structures guaranteeing both protection for the former and an effective adhesion on the latter. This work proposes a method to obtain such result via thermal spray technique on metallic structures, allowing its use in the most severe conditions of corrosion and wear. Since the transmission medium between the structure and the sensitive part of the optical fiber is represented by the fiber coating, three differently coated fibers were used on C-40 steel substrate: polyacrylate, polyimide and ORMOCER. In addition, the use of a primer to improve the bond on the substrate was evaluated. The adhesion between FO and metallic coating is evaluated through optical microscopy (OM) and scanning electrons microscopy (SEM) analysis. The functionality is also verified with both thermal and mechanical tests to calibrate the measuring accuracy. The results indicate that the best combination is that of the polyimide fiber, a zinc primer and aluminum coating. The proven qualities are the adhesion at the interface between the metallic coating and the fiber optics, and the preservation of the structural integrity of the fiber itself and its coating, and a precise measurement of strain acquired by fiber Bragg grating sensors (FBGs). The use of the thermal spray process is thus proved to be a solution for the optical fiber and substrate interaction, since it preserves the integrity of the optical fiber, due to the low temperature of the process, adding the protection that the metallic coating offers as well.

Handling Editor: Maude Jimenez.

Address correspondence to E-mail: daniela.rigamonti@polimi.it

https://doi.org/10.1007/s10853-024-09914-9

Introduction

The application of fiber optics (FO) technology for structural monitoring in civil engineering is increasingly growing in the recent years [1–6]. Indeed, FO accuracy and reliability make it a valid alternative to more traditional sensors. In addition, it might also present improvements: the basic ones are small size, lightness, immunity to electromagnetic interference (EMI) and corrosion; others, requiring a fine design phase, are the possibility of multiplexing (i.e., managing multiple measuring points on the fiber itself operating as a single connection cable) or the use of different measuring techniques depending on the use case, ranging from single-point measurements to integral ones on a large portion of the structure.

Another captivating characteristic of FO is the possibility to insert them within host structures, even though some care toward the quality of the interface is mandatory [7]. This is facilitated for structures that lend themselves well to inserting additional elements, such as composite structures. Conversely, it is far more complex to anchor FO to structures such as metal ones. Various techniques have been tested to embed fiber optics in metals. The main adopted include welding-based methods (e.g., tungsten inert gas welding (TIG) [8] or simple soldering [9]), laser-based additive manufacturing (AM) (e.g., directed energy deposition (DED) [10–12], selective laser melting (SLM) [13–15] and laser metal deposition (LMD) [16]) and ultrasonic additive manufacturing (UAM) [17–21] and [22–25]. Except for UAM, all the listed approaches go through the phase transition to the liquid state of the metal, thus reaching high temperatures. This leads to the need to use fibers with highly resistant metal coatings or to cover the fiber with protective metal layers deposited for example with sputtering or arc-spraying. Zhang and coworkers go so far as to use using sapphire fibers for spark plasma sintering (SPS) [26]. Even so, the high temperatures cause an increase in locally induced thermal stress, with the risk of compromising the quality of the measurement. Moreover, the use of high-temperature techniques is unlikely viable in monitoring existing large structures, since they require complex machinery or inert environments and have high costs. Only a few authors use FO with standard polymeric coatings applying UAM. Chilelli et al. [23] and Schomer et al. [22] use polyacrylate-coated FO and they identify in birefringence-induced noise an indicator of an undersized channel and possibly of poor bond quality. Hehr et al. in 2018 [24] use ORMOCER-coated FO, but they do not discuss bond quality. Again Hehr et al. in 2019 [25] use polyimide-coated FO in combination with a continuous measurement technique based on Rayleigh backscattering instead of FBGs. The quality of the adhesion between the UAM-welded layers is verified, although not around the FO, whose adhesion to the metal part is assessed indirectly by measuring the residual strain around the embedded FO. However, although UAM has been demonstrated as an effective approach to encapsulating polymeric-coated FO in aluminum alloys, it is challenging to achieve a good fiber/matrix bond for high-temperature materials such as steel.

Thus, it is of interest to pursue some economical and adaptable ways to embed FO sensors with standard polymeric coatings into metallic structures with low residue stresses. According to these premises, an adequate thermal spray technique presents itself as a promising alternative [27]. This option is strengthened thinking that the coatings produced by thermal spray techniques are already used to protect metal structures, during their installation or maintenance, so the insertion of the fiber optics would be a value addition. One of the advantages of using thermal spray process instead of using the other cited embedding techniques lies in its versatility. Thermal spray processes are available with a large variety of coatings with different characteristics and costs. According to Qadir et al. [28], the challenges posed by the industrial growth have pushed to develop coatings with specific characteristics suitable for diverse operating conditions and selecting appropriate materials or surface coating technologies can be crucial [29]. Moreover, thermal spray processes are already applied by industry to protect structures from severe conditions of corrosion and wear, so it appears simpler to scale this technique to add FO for monitoring existing large structures, especially considering using mobile spray units and manual application.

Among thermal spray processes, technologies using too high temperature, such as high-velocity oxy-fuel (HVOF) and electric arc, are immediately discarded, since that implies an increased risk of damaging the FO. The limit temperature of standard borosilicate fibers is up to 1200 °C; however, the in-use limit is given by the coating. There are metallic (or experimental) coatings that can withstand temperatures above 1000 °C [30]; however, they are very expensive and thus limited in their practical use. The most common

coating for high temperatures is polyimide, which provides excellent thermal stability and some of the highest operating temperatures for fiber optics: up to over 280 °C of continuous exposure, as well as short-term excursions as high as 400 °C. ORMOCER®-T coated fibers can be used within a wide temperature range up to 200 °C. Polyacrylate is the least resistant from all points of view, mechanical, chemical and thermal, and its operating temperature is below 80 °C. It must also be considered that the temperature of the process is combined with the mechanical stress due to the impact of the particles, although specific studies on the impact resistance of the FO coating are lacking. Conversely, the cold spray [31–33] and combustion wire spray [34, 35] represent the most suitable choices: the temperature is relatively low, and the bonding process is attributed to adiabatic shear instability occurring at the particle–substrate or particle–particle interface due to the high kinetic energy [32]. During impact the solid particles undergo plastic deformation, promoting bonding with target surface. Comparing the two processes, the wire spray process is more advantageous when using optical fiber. In the cold spray process, the material impacts the surface with greater energy. The higher the impact energy, the greater the likelihood that the optical fiber will not withstand the process and will be damaged. The use of the wire spray technique more likely allows the preservation of these fibers because the atomized particles reach the surface with a smaller or less vehement jet [32], and with that the fibers remain in position and intact. For this reason, this technique was chosen for this work. With the combustion wire spray, using a flow of heat (about 3000 °C) produced by the oxidation of a combustible gas, normally acetylene or propane, the wire spray material is melted in a gaseous oxygen–fuel flame. The wire is fed concentrically into the flame, where it is melted and atomized by the addition of compressed air that also directs the melted material toward the workpiece surface [35]. The use of flame does not induce high temperatures in the coated substrate. This is mainly due to the strong difference between the mass of the coated substrate (cold) and the mass of the coating itself (hot). The microstructure obtained in this process is quite different. According to Talib et al. [35], the molten or semi-molten material impacts on the substrate surface with their specific kinetic energy, then it rapidly solidifies, and forms splats. Each splat is a single impacted particle in a "pancake-like" shape, and the coating is formed by the overlapping splats, where the new ones solidify and interlocked each other.

The idea here presented is to apply the thermal spray technique to embed polymeric-coated FO with inscribed FBGs on a steel substrate. The target is many-sided: ensuring good adhesion, promoting an efficient sensing, maintaining low invasiveness of the FO. From the objective of creating a well-unified part comes the requirement to guarantee a good condition of the protective coating of the FO, which guarantees that its cores and cladding are also intact and that deformations are well transferred from the metallic structure to the FO core.

A stage of analysis regarding the combination between different types of sprayed coatings and fibers coating was mandatory. The adhesion between FO and metallic coating is evaluated through optical microscopy (OM) and scanning electrons microscopy (SEM) analysis. The functionality is also verified with both thermal and mechanical tests to calibrate the measuring accuracy.

Materials and methods

Thermal spray parameters and FOs data

The substrate for the thermal spray (combustion wire spray) deposition was a C-40 steel plate with 20 μm grit Al2O3-blasted surfaces. In general, considering the relatively low mechanical proprieties of the polymeric coating of the optical fiber, a conservative choice in terms of thermal spray technique and materials is made. The material selected for the metallic coating layer is aluminum at 99, 5%. In some cases, an intermediate binder (primer METCO—405 or zinc) was firstly applied to increase the adhesion of the metallic coating. Compressed air was used to accelerate and atomize the powder. A complete description of the process parameters is detailed in Table 1.

The fiber coating is a polymeric layer applied externally to the optical fiber to provide mechanical protection to the glass, whose cladding diameter is 0.125 micron in this case. The most common coating in the FO industry is polyacrylate, usually deposited in two layers (typically known as primary and secondary coatings, hence the wording "dual acrylate"). This is also the one with the lowest mechanical, chemical and thermal properties, so other coating materials such as high-temperature acrylate (HTA),

Table 1 Parameters of thermal spray deposition process

Material	$O_2(psig)$	$C_2H_2(psig)$	Deposition velocity(*lbs/hr*)	Deposition distance(*inch*)	Coating flow(ft^2/*hr*)
Aluminum (coating)	43	40	12	5–8	833
Zinc (primer)	45	40	32	5–8	625
Metco–405 (primer)	44	39	5	5–8	111

Table 2 Highlights of the different configurations of the produced specimens

Condition	Primer	Thickness of the aluminum coating	FO coating	Dimension of the C-40 substrate plate (mm)	V-groove
1	METCO–405	0.2 mm	Polyacrylate	60×130, thickness 120	Yes
2	METCO–405	0.2 mm	Polyacrylate	60×120, thickness 20	No
3	Nickel and chromium, namely *bondrite*	0.2 mm	Polyacrylate	60×130, thickness 3	No
4	zinc	0.2 mm	Polyacrylate	60×200, thickness 20	No
5	zinc	0.4 mm	Polyimide	60×10, thickness 3	No
6	zinc	0.8 mm	ORMOCER	60×10, thickness 3	No
7	Nickel and chromium, namely *bondrite*	0.8 mm	ORMOCER	60×10, thickness 3	No

polyimide (PI), metals or carbon are also applied to the optical fibers in single- or dual-layer structures depending on the applications and environmental conditions where the fibers have to be used. Another patented coating is ORMOCER (short for organic modified ceramics) that describes a group of hybrid polymer materials providing very strong adhesion with glass and good general protective properties. In this work, three types of coatings are put on trial: the most common polyacrylate, the unique ORMOCER and the polyimide, known for its hardness and good chemical/thermal resistance.

Another aspect, which might appear paltry only at first, is the thickness of the substrate sample. Indeed, the fiber is deteriorated not only by the mechanical action of the particles, but also by the high temperatures reached during the process. Besides the parameters of the thermal spray, another cause of the temperature increase might also be the not adequate heat dissipation provided by the underlying specimen. The consequence is the degradation and, eventually, the melting of the FO polymeric coating with a consequent reduction of its protective properties toward the glass core.

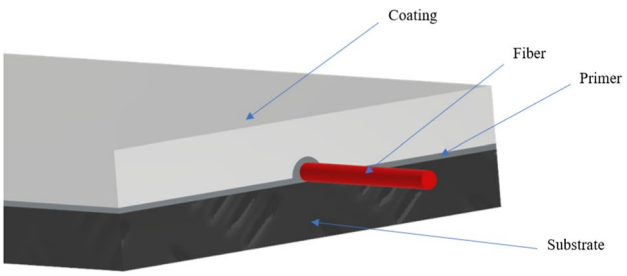

Figure 1 Sketch of the specimen configuration with primer layer and no v-groove.

To give a schematic overview of the attempted combinations, the material configurations are detailed in Table 2. To create a seat that can accommodate the FO and help its positioning, for one sample (condition nr. 1 in Table 2) straight v-grooves are engraved using a milling machine on the surface of the specimen. Figure 1 sketches the configuration of the specimens without v-groove, while in Fig. 2, a picture shows the aspect of the specimen in condition nr. 1, with groove.

To validate the integrity of the fiber after the production process, a simple check is performed using

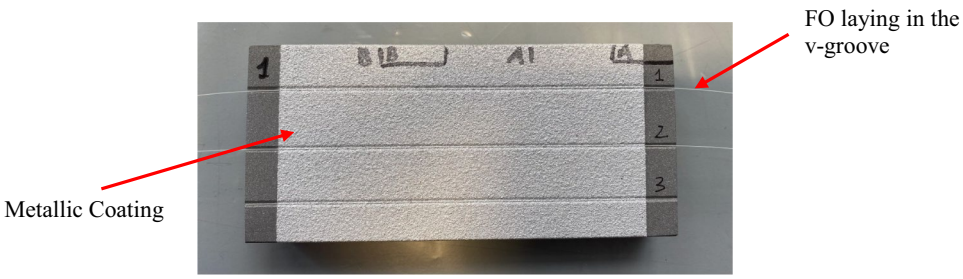

Figure 2 Aspect of specimen condition 1, with groove.

a Fluke Networks Visual Fault Locator (VFL, Fig. 3). This instrument generates a signal in the visible range (a red light), so that breakages in the FO can be easily identified. If the light is visible at the opposite end of the fiber with respect to the one connected to the source, then no damage has been produced and the signal can be correctly transmitted. This test made it possible to verify that for each of the produced specimens the thermal spray process performed with the set parameters guarantees the integrity of the optical fiber core, before moving on to subsequent analyzes.

Thermo-mechanical decoupling

On two samples produced as per configuration 5—which will prove to be the best one after the technological assessment–an additional action was taken during the preparation phase: a capillary tube (steel, outer diameter 0.4 mm, inner diameter 0.15 mm, hereafter abbreviated as CT) is inlaid over one of the two sensors to allow the decoupling of the thermal and mechanical effects. This technique [36] leaves the sensor unconstrained inside the tube, so it is isolated from mechanical strain, while it is subject to temperature change with only a slightly different sensitivity with respect to the sensor embedded in the metallic coating. In this way, by writing the system of equations describing the sensor response to the strain and temperature fields, a well-conditioned coefficient matrix is obtained which allows it to be inverted to decouple the solicitations.

$$\begin{bmatrix} \Delta\lambda_1 \\ \Delta\lambda_2 \end{bmatrix} = \begin{bmatrix} C_{\varepsilon 1} & C_{T1} \\ 0 & C_{T2} \end{bmatrix} \begin{bmatrix} \Delta\varepsilon \\ \Delta T \end{bmatrix} \quad (1)$$

The procedure to add the CT (Fig. 4) is conceptually trivial, but delicate in practice. Two drops of glue must be applied to fix the tube to the fiber and to seal the tube itself. During this operation, great care must be taken to guarantee that the temperature sensor is completely included in the CT, and it does not get stuck, even partially, by the glue applied to seal. The needed care was aggravated, in this case, by the proximity of the two sensors, whose distance is only 5 mm. The consequences are illustrated in Fig. 5. If no further precautions are taken (Fig. 5a), the first part of the fiber outside the CT would bend to accommodate the step caused by the thickness of the CT, which, although small, is not negligible. The space created in this small volume between the fiber and the substrate is a crucial area, because it distances the FBG from the substrate and it prevents the correct deposition of the thermal spray coating as well. The result is that the external sensor that must measure the deformation

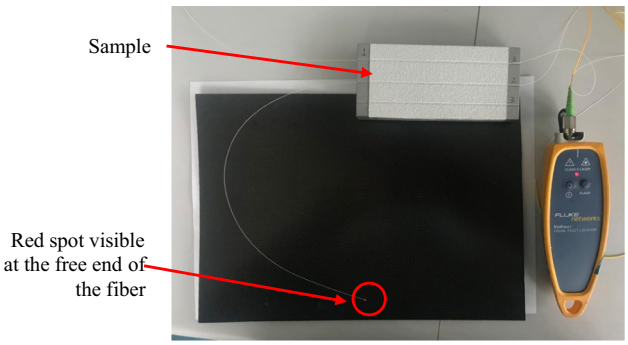

Figure 3 Aspect of the test done with the visual fault locator after thermal spray process.

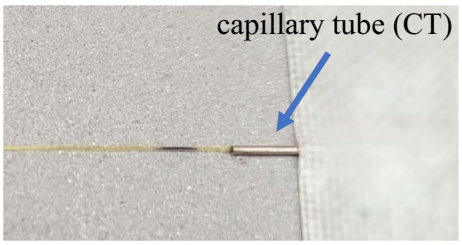

Figure 4 Detail of the capillary tube (CT). On the left is the sensor that will be coated (marked in black just outside the tube); on the right is the isolated one (inside the tube).

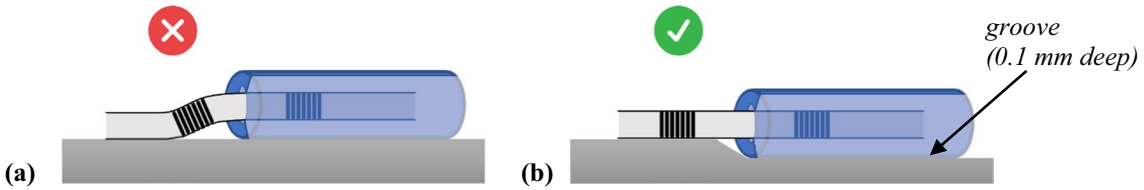

Figure 5 Installation of the capillary tube (CT) for decoupling: **a** incorrect without groove and **b** correct.

is not adequately integrated, thus being unable to acquire information effectively. When the fiber thus arranged is subjected to load it is easy to assume that not only the measurement is less accurate, but also that the separation of the fiber can propagate at the interface with the substrate, aggravating the situation with subsequent cycles or increasing the load. To prevent this from happening, a slight groove 0.1 mm deep is made in the substrate to house the CT and keep the fiber straight (Fig. 5b).

The mechanical coefficient was taken as the theoretical value $\lambda_B(1-p_e)$. To proceed with the decoupling, it was first necessary to carry out a calibration to measure the thermal coefficients. This was done on the complete samples (with fiber already embedded) rather than on the fiber alone, because the mechanical and thermal coefficients are influenced by the CTE of the host material. Strictly speaking, the stress/temperature variations also produce a change in the refractive index of the optical fiber and thus in the wavelength. However, this procedure aims at directly calibrating the multiplicative factors between the wavelength variations and the strain and temperature fields. There was no need to evaluate specifically the effect on the physical coefficients on which these factors depend (e.g., the thermo-optical one).

Two samples, together with an unembedded sensor of the same type, were placed in an oven with programmable temperature ramp (Mazzali Thermotest 300 °C 100 L). Three thermocouples were applied very close to the sensors with metallic adhesive tape (see Fig. 6). Both the FBG sensors measures, and the temperatures were collected simultaneously.

Validation methods

The validation of the quality of the technique was approached from two points of view. The first was purely technological and it was intended to study the effectiveness of the integration. To this aim, optical fibers without sensors would suffice for the microscopic analyzes and permanent bending tests performed. The second methodology is intended to verify the monitoring performance of the sensors and therefore requires fibers with inscribed FBGs. In this phase, both manufacturing and bending tests were monitored.

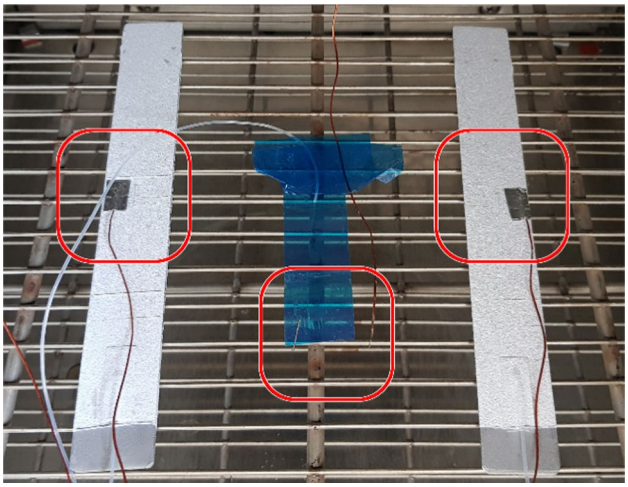

Figure 6 Two samples and a free FBG on oven grid for temperature calibration.

The purpose of the technical assessment was to evaluate the twin invasiveness of adding the FOs. Firstly, we intended to verify that the thermal spray process does not damage the optical fiber that would cost its performance as a sensor. Secondly, it is also important that the optical fiber does not reduce the quality of the deposited aluminum layer, especially if this has not only the function of making the optical fiber adhere to the substrate, but also that of protecting the substrate itself (for example, typically, from corrosion). To carry out this analysis, initially the first aspect was evaluated, considering it the most critical point of the technique. Downstream, the second aspect was tested only on the combination found to be the best among those shown in Table 2. To check the first aspect, the microstructural and morphological characteristics of the FO coating, the metallic sprayed coating and their interface after the process were

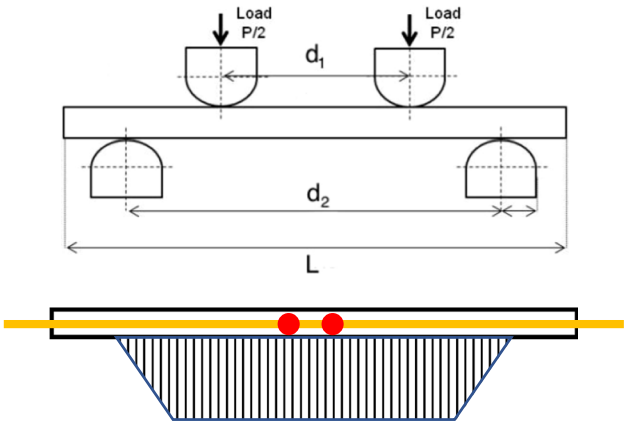

Figure 7 Setup for the four-points bending test.

analyzed. Three sample cross sections for each fiber were observed. Both an optical microscope (Nikon SMZ-U) and a scanning electron microscope (Hitachi Tabletop Microscope TM3000) were used, with magnifications ranging from 100x to 500x. During the cutting performed for obtaining the cross section is important to avoid damaging the coating and the FO. To this aim, the surface of the sample was covered with two-component epoxy casting resin, taking care not to create bubbles. The cuts were made with a miter saw with a water-cooled diamond blade. Then, the sections were prepared by standard metallographic techniques, sanding and polishing, without etching. Uniformity in the characteristics of the different sections along the same fiber was observed, so only the most significant images have been reported in the paper for brevity. As for the second aspect, i.e., the invasiveness of the FOs on the aluminum coating, the first bending test indicated in the ASTM B 571–97 Standard (Practice for Qualitative Adhesion Testing of Metallic Coatings) was applied. Three samples were produced with the parameters of condition 5 and then analyzed to check the invasiveness of the FOs on the aluminum coating through the bending test. One is a reference sample and thus no FOs were introduced. The other two have a polyimide-coated fiber: one with the FOs in the same direction of the passes given with the wire spray gun, the other with the fibers placed transversely, so that the jet of particles impacts the side of the fiber itself. The samples were then bent 180° on a mandrel (until their two legs are parallel) with the coated surface on the tensioned side.

Performance proof included manufacturing monitoring and four-point bending, as depicted in Fig. 7.

Table 3 List of specimens with FBG sensors produced and tested

Samples ID	Sensors configuration in the samples
01	1 FBG directly embedded + 1 FBG in CT
02	1 FBG directly embedded + 1 FBG in CT
03	2 FBGs directly embedded

During the manufacturing process of the specimens with the CT, the fiber was connected to the Micron-Optics SM130 interrogator, allowing a live acquisition of the thermal spray process. The presence of the CT allowed the decoupling of thermal and mechanical stresses. Same samples were employed in a four-point bending test. The machine MTS 858 MiniBionix was used with 1 mm/min compression speed and 10 Hz data acquisition frequency. The distances between the two upper and lower supports were set at 60 mm and 160 mm respectively. Both the FBG sensors measures, and the bending machine parameters were collected. The trend of strain is investigated over the time at different magnitudes of force applied corresponding to three maximum values of strain: 1000 με, 2000 με (repeated twice) and 2400 με.

In Table 3 is summarized the list of the samples produced with FBG sensors.

Results of the technological assessment

Optical analysis

The adhesion between the fiber and the substrate via thermal spray is the crucial point of a suitable design, but the FO must remain intact to guarantee the correct functioning. As can be seen in Fig. 8a, the solution that provides the groove as a method for maintaining the fiber in the desired position (condition 1 in Table 2) is not an acceptable solution. The micrograph shows how the coating has deteriorated to the point that it is no longer able to cover and protect the core. Conditions 2 and 3 also highlight the deterioration of the polyacrylate coating: it is evident how it has been stripped away—and possibly also softened due to the temperature—to the point that it has become a foreign body to the fiber itself (Fig. 8b and Fig. 8c). Among the combinations using polyacrylate coating, only the condition 4 (zinc primer without V-groove) evidently allows to preserve the

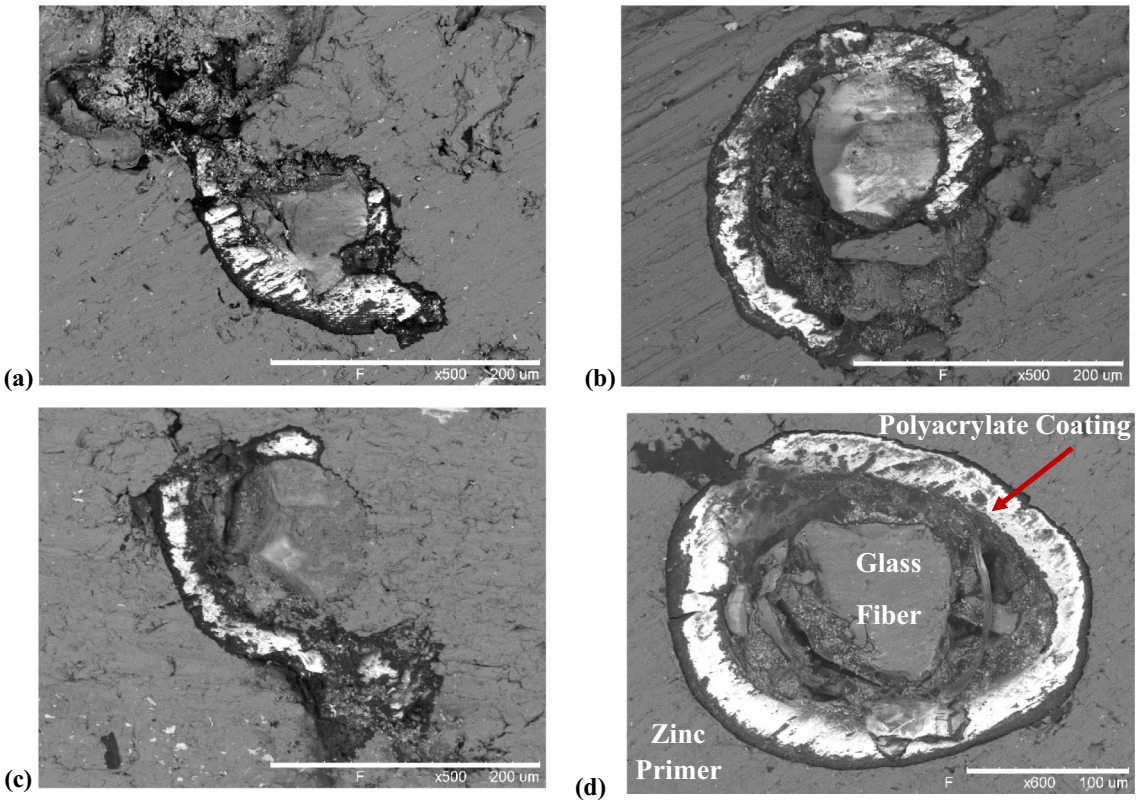

Figure 8 nSEM micrographs exhibiting the aspect of FOs with polyacrylate coating after thermal spray process. Conditions with reference to Table 2: **a**-1, **b**-2, **c**-3, **d**-4.

integrity of the fiber (Fig. 8d). This condition shows the particularly interesting effectiveness of the use of zinc, which proves suitable to protect the polyacrylate fiber that was instead completely damaged in the previous conditions. Zinc shows protective effect against cladding, which was found to undergo only a slight deformation. The effectiveness of zinc is to be found in its metallurgical properties: it is a low melting and very ductile metal. Thermal spray coatings rely primarily on a mechanical or interlocking bond between the coating and substrate. In this case, during the deposition process, the particles deform and adapt to the fiber's shape, allowing both the required adhesion, even with a poor coating like polyacrylate, and a reliable anchoring point for the subsequent layer of aluminum. Moreover, zinc primer has a thickness of only 0.1 mm, which should ensure a good ability to transfer information from the substrate to the fiber.

Starting from the results obtained in this first bunch of attempts on polyacrylate, other combinations were explored, in particular, the possibility of using different materials for the coating: polyimide (condition 5) and ORMOCER (conditions 6 and 7).

In Fig. 9 (condition 5: polyimide and zinc primer), it is possible to notice how the fiber remains in good condition. The good adhesion of the fiber is ensured using the zinc primer. Moreover, also the adhesion with the aluminum which covers the specimen appears of good quality. By using this solution, both the goals of a good adhesion and the preservation of the integrity of the fiber are achieved. In fact, the temperatures reached during the manufacturing process are well below the glass transition temperature (Tg) of the polyimide coating (above 300 °C) and the impinging zinc does not scratch the surface.

Conversely, the combination between the same parameters of the thermal spray process and the ORMOCER fiber gives very bad results: although the fiber is not damaged at all by the process, it highlights a very poor adhesion, and it does not even stick to the substrate (Fig. 10). To face this problem, a different primer was tried: *bondrite*. It should increase the quality of the adhesion of the aluminum later deposited,

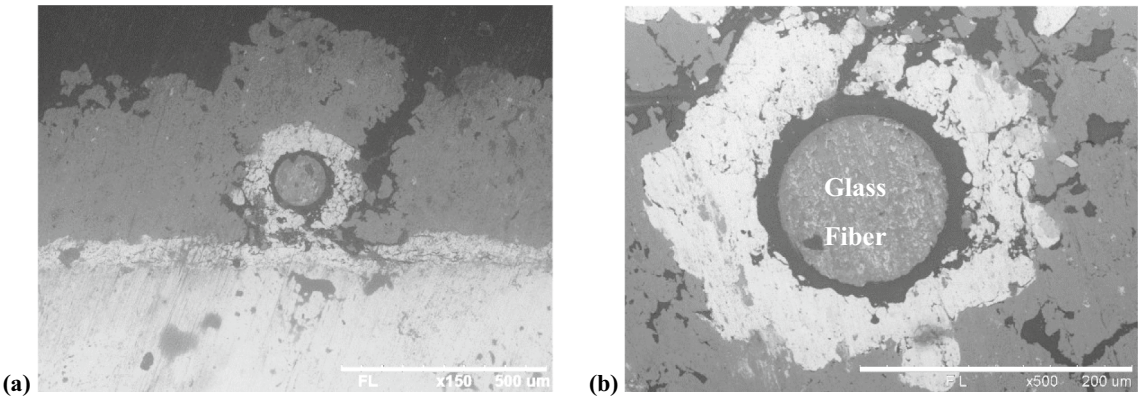

Figure 9 SEM micrographs exhibiting the aspect of FOs after thermal spray process, in condition 5 with reference to Table 2 (polyimide and zinc primer).

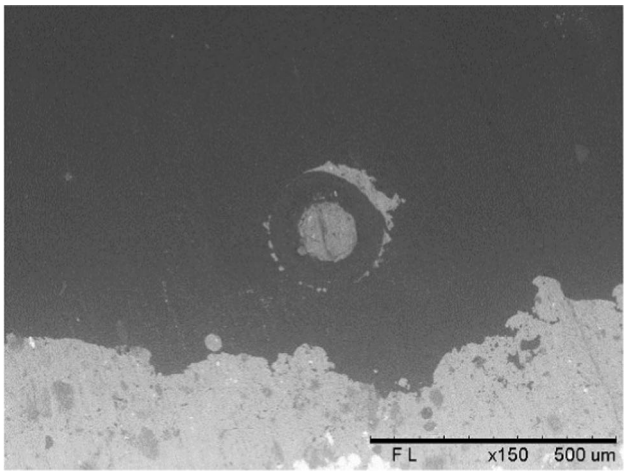

Figure 10 SEM micrograph exhibiting the aspect of FOs after thermal spray process, in condition 6 with reference to Table 2 (ORMOCER and zinc primer).

but also in this case the coating made of ORMOCER showed a poor adhesion with the metallic material, not allowing a good embedding of the fiber. Anyway, in both cases the deterioration suffered by the fiber results limited.

Summarizing: the polyacrylate coating confirms its poor mechanical properties and no condition can preserve the FOs adequately; the option of ORMOCER coating must be discarded since no adhesion with the substrate is confirmed, despite the good mechanical response to the process; the polyimide coating represents the most suitable option among the presented, showing adequate mechanical resistance and perfect adhesion to the substrate via zinc primer (Fig. 11). These samples were then subjected to the following step of the technological assessment, i.e., the adhesion testing of the metallic coating. The results indicate that the thermal spray process is a solution to increase the wear and corrosion resistance [16, 17] of FO in more severe environments, maintaining their operational characteristics that will be demonstrated in the analyses that follow. The presence of few defects in the metallic coating (such as oxides and pores, inherent to this process [18]) which will allow a greater adhesion between the metallic coating and the Zn coating should be noted.

Permanent bending test

Looking at Fig. 12a can be noticed that cracking occurs in the bend area of the reference sample. Cracks are normal and not indicative of poor adhesion unless the coating can be peeled back with a sharp instrument. In this sample, these are superficial and do not propagate into the substrate. In the sample with fibers parallel to the direction of the passes (Fig. 12b), these cracks are deeper with respect to the reference sample, but still no peeling or flaking of the coating from the substrate can be observed, which would be evidence of poor adhesion. This, on the opposite, occurs with the sample in which FOs are transversal (Fig. 12c). Here, the cracks opened on the line where the fibers are positioned act as a trigger point for the lifting of the coating. Where it was fractured, a blade was used to attempt to lift off the coating, which could in fact be easily removed proving the poor adhesion. Despite its small size, the FOs might create a shaded area for the sprayed particles, generating this "trigger line" for flaking. This is an important indication that the

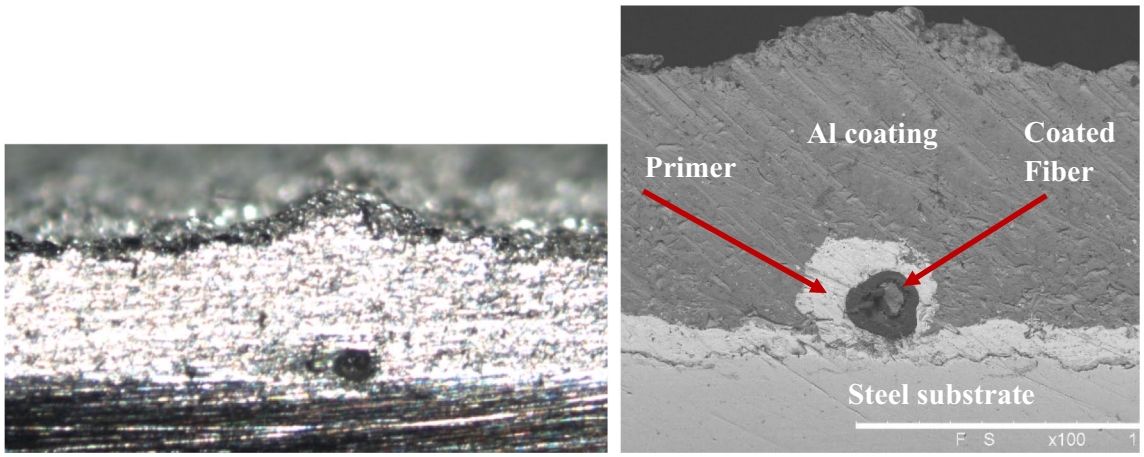

Figure 11 Optical micrograph **a** and SEM **b** micrograph reveal the excellent adhesion and no defect of FOs after thermal spray process with polyimide coating and zinc primer (condition 5).

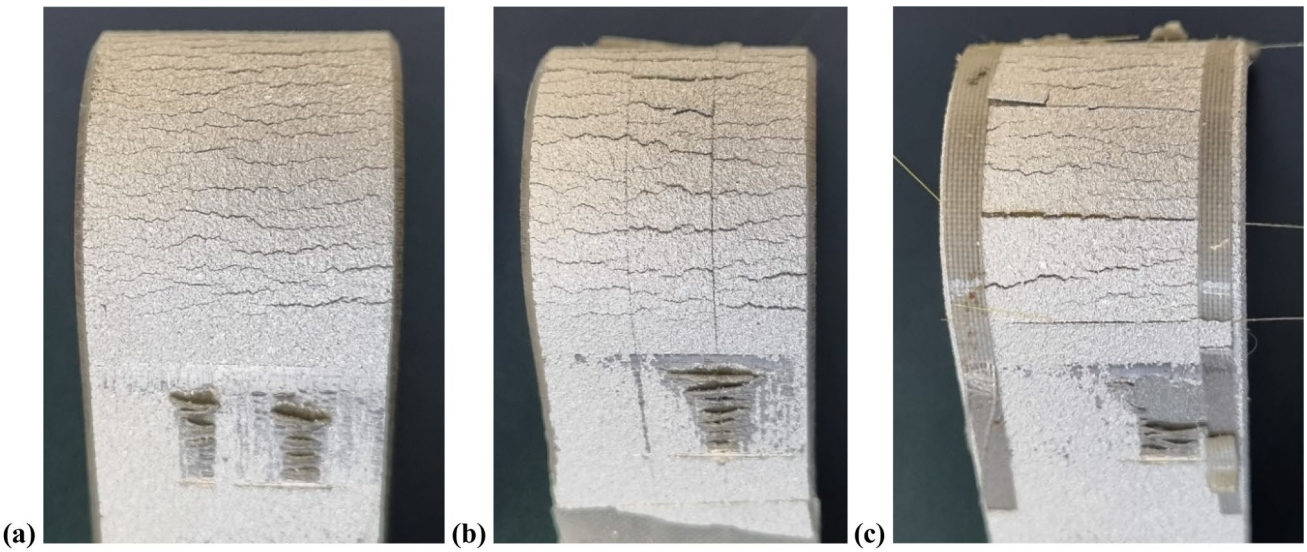

Figure 12 Pictures of the samples after the bending test (according to ASTM standard). **a** Reference sample with no fiber, **b** fibers parallel and **c** fiber transversal to the direction of the passes.

thermal spray technique is effective, but that attention to the position of the optical fibers must be paid during the coating application phase, to avoid adhesion reduction, see Fig. 13.

Results of the performance verification

Temperature decoupling and thermal strain

For the fiber that is not embedded in any sample (Fig. 14), the two FBGs exhibit the same response due to the same coefficient of thermal expansion (CTE), which is that of the fiber itself. There is a slight delay of the response of the sensor inserted in the CT due to the thermal insulation, which also causes a thermal hysteresis that cuts the thermal fluctuations detected

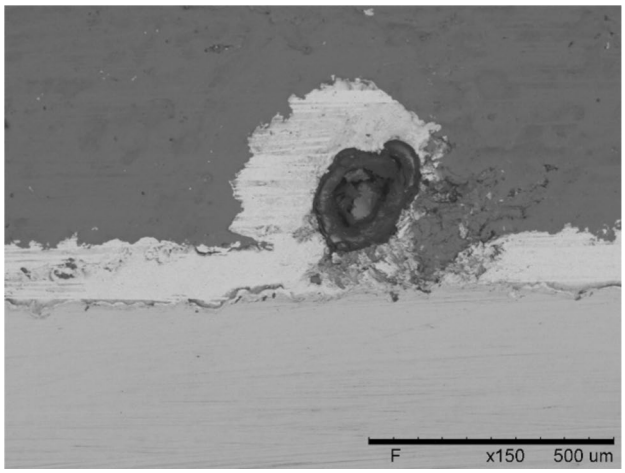

Figure 13 SEM image of the section of the fiber transversal to the direction of the passes.

by the thermocouple. The higher noise of the free sensor signal is due only to the vibrations of the oven fan during cooling.

In both the samples where the fiber is embedded through thermal spray (Fig. 15), it can be noted that the variation in wavelength produced on the sensor embedded in the aluminum layer ("embed. sensor") is greater than that of the free sensor ("free sensor" in Fig. 14). This is a direct consequence of the CTE of the metal and the transfer of its expansion to the optical fiber. This is also a nice indicator of the good adhesion of the FOs to the metal sample and a proof of the fact that the thermal calibration is to be carried out necessarily on the sensor joined to the host material. The sensors in the CT have a different response for the two samples. One of the two has values close to those of the free fiber (Fig. 15b vs. Fig. 14), while the other has higher wavelength variations (Fig. 15a). This too is indicative of the fact that probably, in Sample 1 (Fig. 15a), the sensor is not completely free inside the CT, but has been partially bound by the glue. This reduces the effectiveness but is not very critical, because the possibility of decoupling is still guaranteed if the multiplicative coefficients of the two sensors are sufficiently different.

The resulting coefficients $\Delta\lambda/\Delta T$ are calculated with a linear regression for each sensor of each sample (Fig. 16) and are summarized in Table 4. The average value for free and isolated sensors is about 0.011 nm/K and it more than doubles coming up to 0.025 nm/K for the embedded sensors.

Manufacturing monitoring

In Fig. 17, the wavelength shift of the two FBG sensors is shown, as acquired during thermal spray manufacturing process (when the mechanical and thermal actions are still uncoupled). Each of the peaks coincides with a passage of the sprayed thermal jet hitting the fiber. From the curve, four different deposition peaks are visible: the first two (within the first minute) are when the primer is deposited, the next two are related to the deposition of first and second aluminum layer. Between two subsequent deposition peaks, the typical trend of a convective thermal dissipation is observed. Even with no decoupling, it is clear that peaks intensity is related to the maximum temperature reached. The ones related to zinc are lower since it has a lower melting point than aluminum. Moreover, among the two aluminum-related peaks, the second

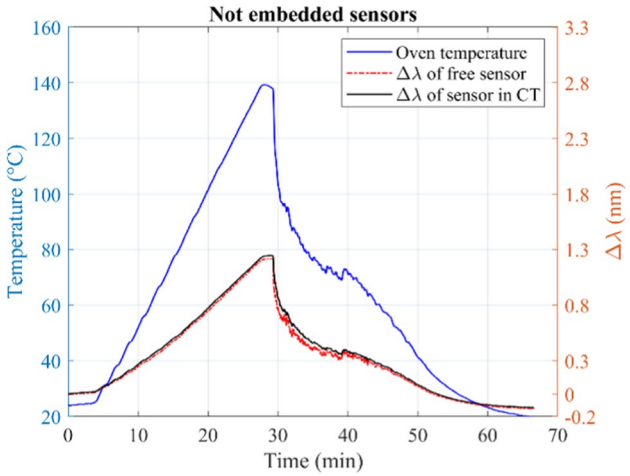

Figure 14 Wavelength variation over time due to a temperature cycle for the sensor not embedded in any sample (one free and another incapsulated in the CT).

one is higher because more cycles of deposition are done in a very small amount of time. Besides, the negative wavelength shift sensed by the embedded FBG is due to the fact that once the fiber is bound to the substrate (that occurs in hot conditions) its response to thermal changes follows thermal contraction of the metal (which is cooling), resulting in a lower strain with respect to the initial condition measured by the FBG. All these considerations are confirmed once the two effects have been decoupled (Fig. 18).

Looking at the detail of the peaks (Fig. 19), each of these is composed by several sub-peaks as direct

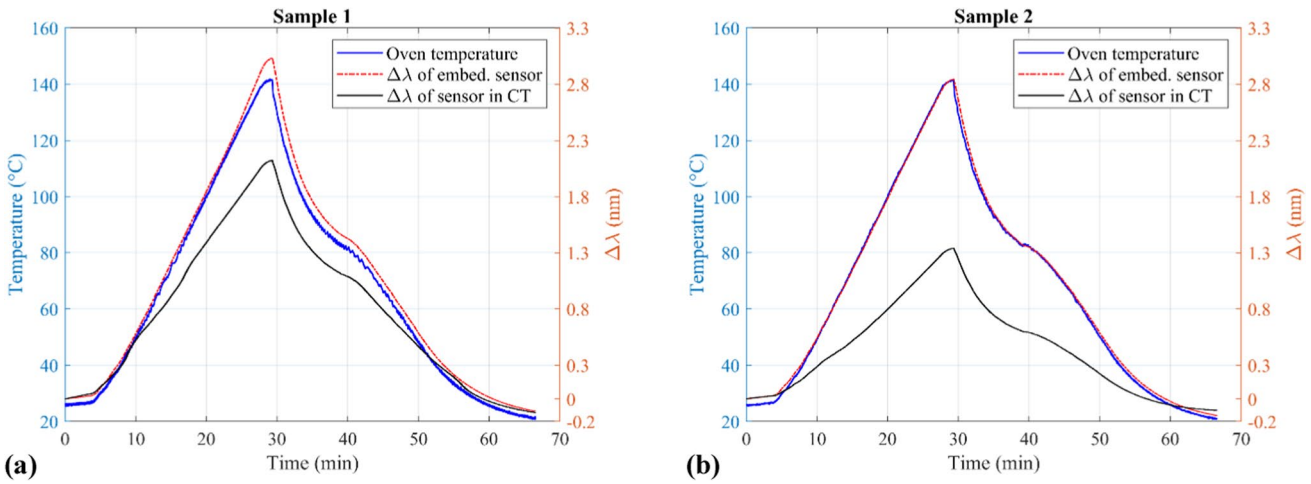

Figure 15 Wavelength variation over time due to a temperature cycle for the sensors embedded in **a** sample 1 (fully embedded) and **b** sample 2 (incapsulated in the CT).

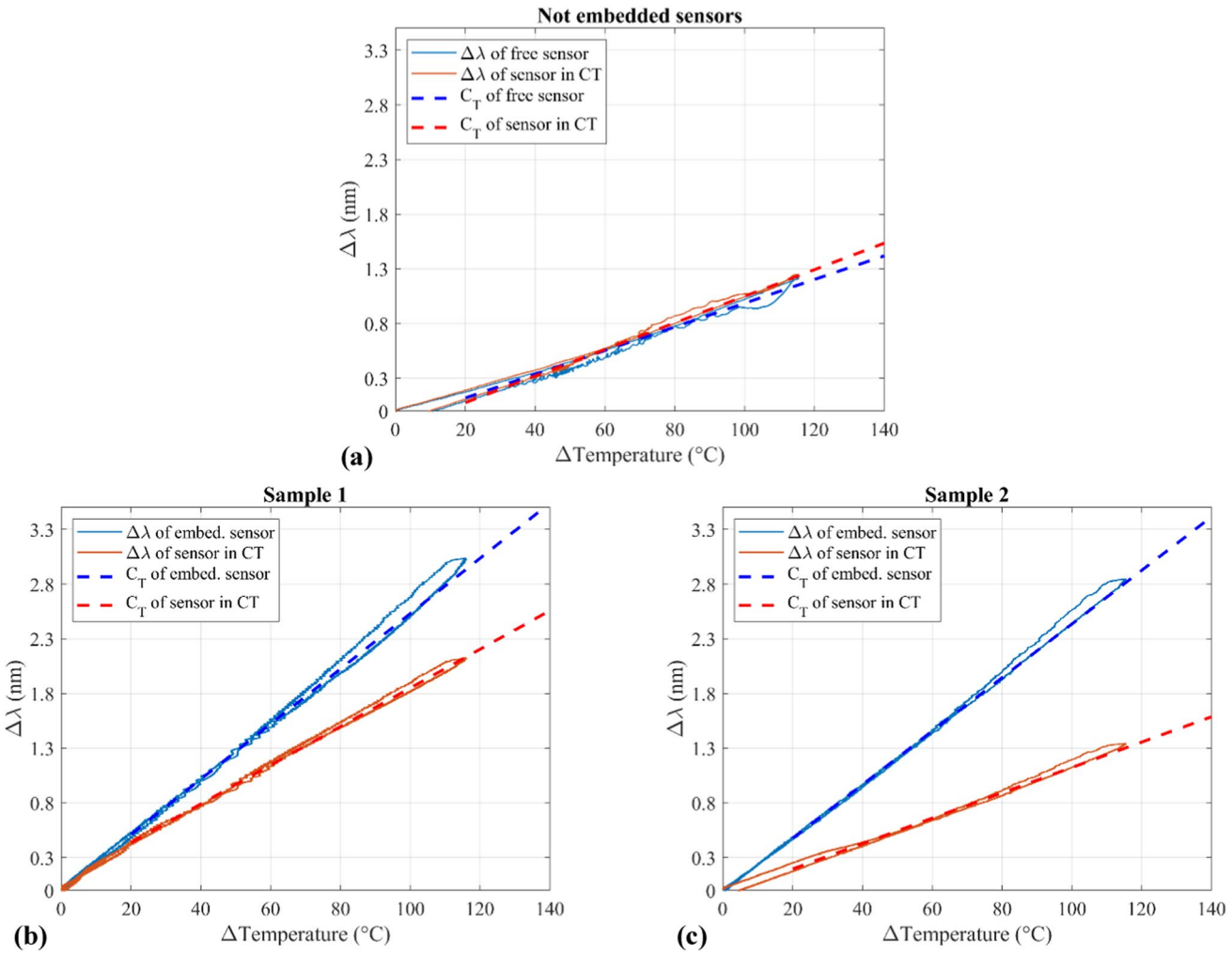

Figure 16 Linear regression of the wavelength shift over temperature. For the sensor not embedded in any sample **a**, for sample 1 **b**, and sample 2 **c.**

Table 4 Sensitivity coefficients from linear regression

Δλ/ΔT	Not embedded (nm/K)	Sample 1 (nm/K)	Sample 2(nm/K)
Free/embedded	0.0108	0.0252	0.0245
Inside CT	0.0121	0.0177	0.0116

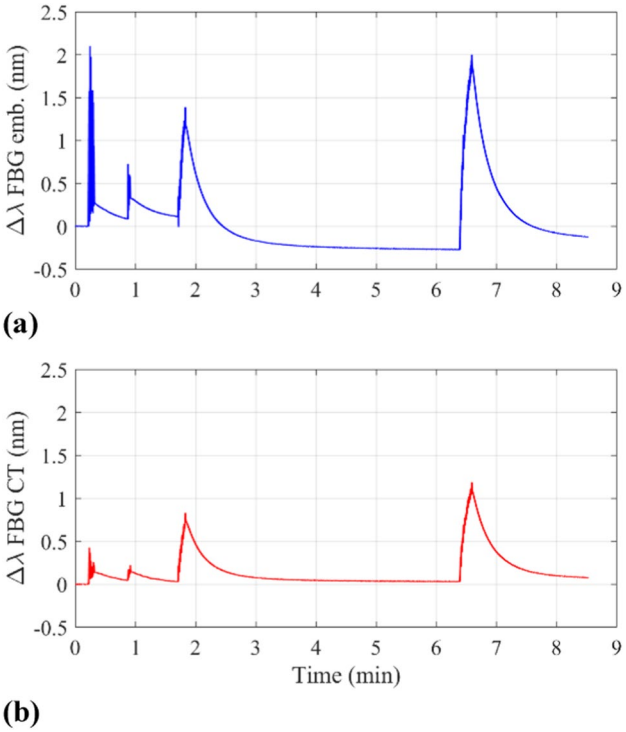

Figure 17 Wavelength shift of the embedded sensor a and the one incapsulated in the CT **b** as acquired during thermal spray manufacturing process.

consequence of deposition process, consisting in the application of a series of subsequent coats of material in rapid succession. Number of coats can be recognized on the curve: seven coats for the first cycle (Fig. 19a, 0.2–0.3 min) and four for the second (Fig. 19a, around 0.9 min). Moreover, the strain is proportional to the strength of impacts: during the second cycle, the detected intensity is lower than the first one because there is not a direct impact, having already deposited a first layer of metallic material. Eight different subpeaks are countable during the first cycle of deposition of aluminum (Fig. 19b, 1.7–1.85 min), representing the eight coats of aluminum deposited in this phase. (A freeze-frame of the deposition process is catched in Fig. 20)

Four-point bending mechanical monitoring

The bending test for a specimen with two embedded sensors (Sample 03, Fig. 21) and another with the CT (Sample 02, Fig. 22 and Fig. 23) are presented.

For the first, the test at maximum strain is reported in Fig. 21. The strain trend labeled as "MTS" is not a direct measure (e.g., from a strain gauge), but is calculated from the force using the theoretical formula for four-point bending (see also Fig. 7):

$$\varepsilon = \frac{1}{E}\frac{M_x y}{J_x} = \frac{1}{E}\frac{-F_{MTS}d_1}{2}\frac{12}{bh^3}\frac{h}{2} = -\frac{3F_{MTS}d_1}{Ebh^2}$$

The strain measured with FBGs proves to be accurate when compared with the one calculated from MTS displacement and load values. The accuracy and

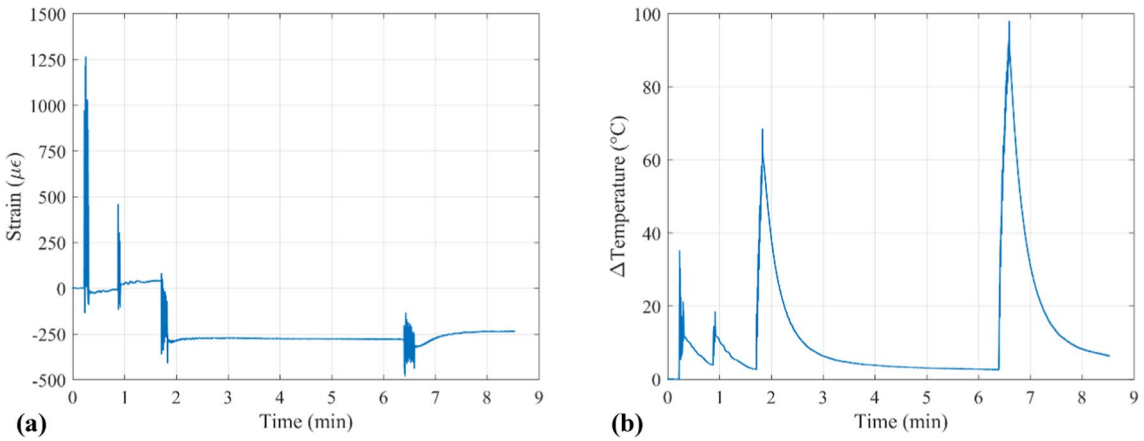

Figure 18 Strain **a** and temperature **b** trend during the thermal spray manufacturing process.

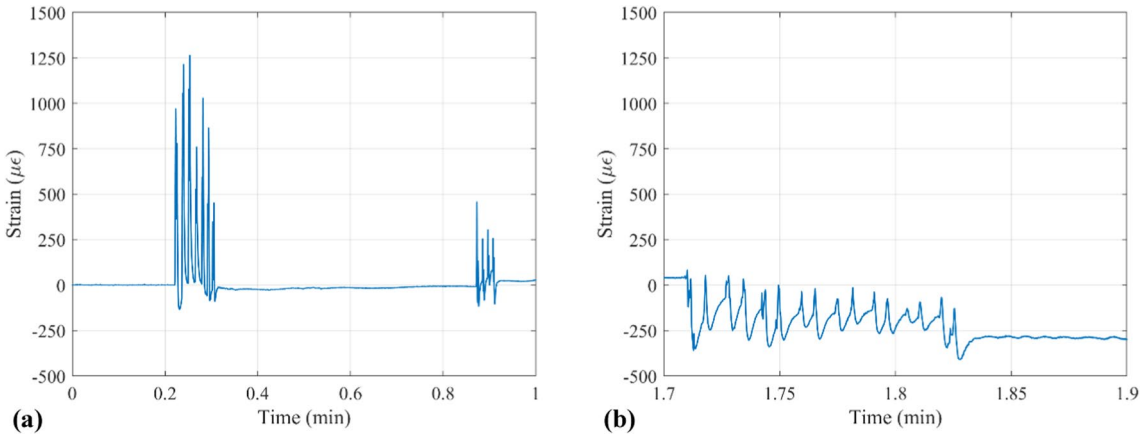

Figure 19 Detail of the mechanical strain induced by the application firstly of the Zn primer **a**, and then of the first coat of Al **b.**

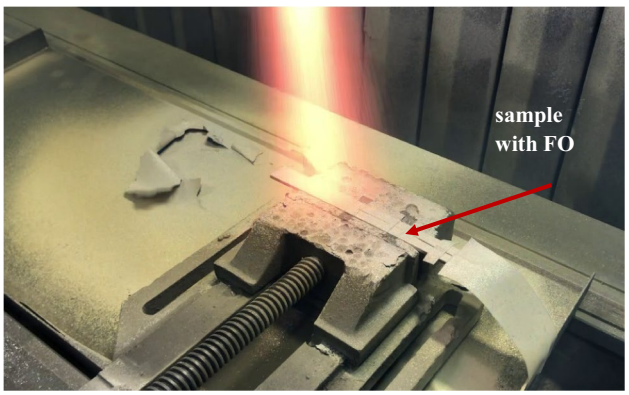

Figure 20 Freeze frame catching a moment in which the thermal spray jet impacts the sample with FO.

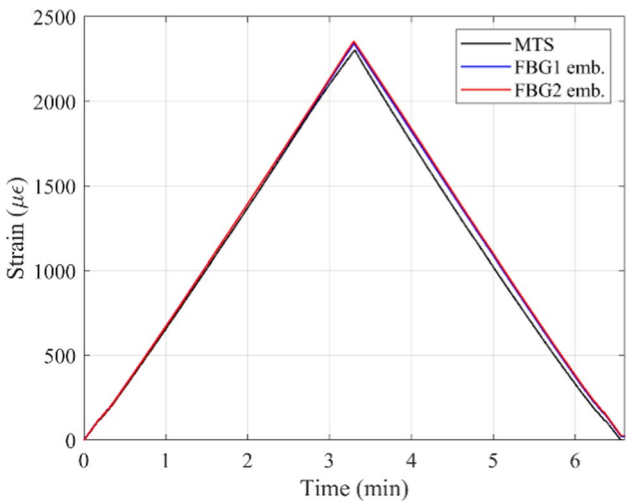

Figure 21 Strain over time for the sample with two FBGs embedded (Sample 03).

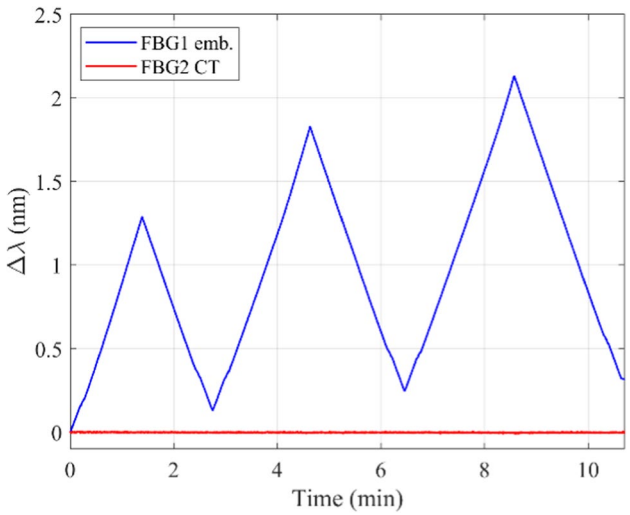

Figure 22 Wavelength shift of the two sensors just as acquired during thermal spray manufacturing process (Sample 02).

the repeatability of the measurement suggest a good adhesion of the thermal spray coating to the fiber, supporting the quality of the configuration adopted.

For the second specimen, the wavelength shift detected by the FBG enclosed in the CT is null, proving the proper mechanical isolation provided by the technique (Fig. 22). In fact, test was carried out at constant temperature so that no wavelength changes due to temperature were expected. The strain and temperature field reconstructed from the decoupling system are in Fig. 23. FO strain calculated from decoupling and MTS one estimated using four-point bending formula are compared in Fig. 23a. The FO measure is very reliable also for this second specimen, up to being more accurate than the deformation value obtained from the MTS load. Indeed, FO detects a

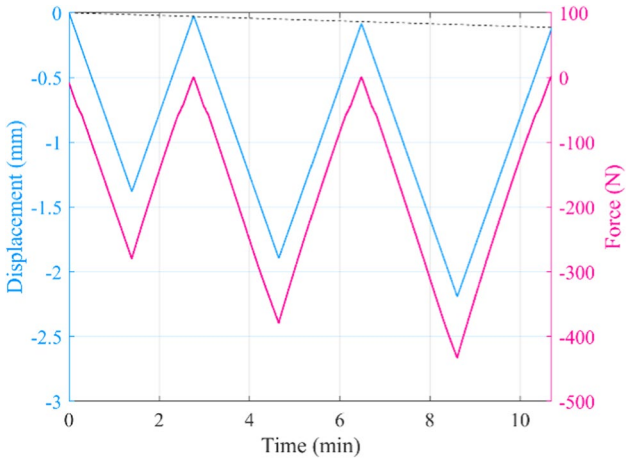

Figure 23 Data acquired by the MTS machine: crossbar displacement and load.

permanent deformation that is suggested by the displacement of the crossbar, whereas it is not detectable by the force that returns to zero after each cycle despite permanent deformation (Fig. 24). This also proves the FO to be comparable to a strain gage local measurement.

Conclusions

In this work, FOs are embedded on metallic structures via thermal spray. This additive manufacturing technique allows depositing a layer of metallic coating over the fiber, fixing it on the substrate, which must be properly treated. The validation of the quality of the technique was approached from both technological and functional points of view.

First technological evaluation was related to the influence of the process on the microstructural and morphological characteristics of the FO coating, explored using optical and scanning electron microscopy. As a result, the FO with polyimide coating represents the most suitable option among the presented, with good mechanical response to the stresses and a perfect adhesion on the substrate via primer (zinc). Conversely, the combination between the same parameters of thermal spray process and the ORMOCER fiber gives the worst results because of poor adhesion. Another outcome is that a flat sanded surface is the best preparation for the substrate. A twin technological aspect relates to the effect of the presence of the fiber on the quality of the deposited aluminum layer. The presence of the fiber, despite its small size, was found not to be so irrelevant. If positioned transversely to the jet of particles, it might create a shaded area for the sprayed particles, generating a "trigger line" for flaking. This is an important indication that attention to the position of the optical fibers must be paid during the coating application phase, to avoid adhesion reduction.

The monitoring performance of the sensors was tested both during manufacturing and four-point bending. The detail and the accuracy of the measurements prove that the manufacturing process does not affect the functioning of the sensors and that the adhesion of the sensor to the structure obtained with the thermal spray is precise.

The effect of temperature has also been considered. This can be effectively decoupled with a capillary tube (CT) technique, even though its invasiveness is not

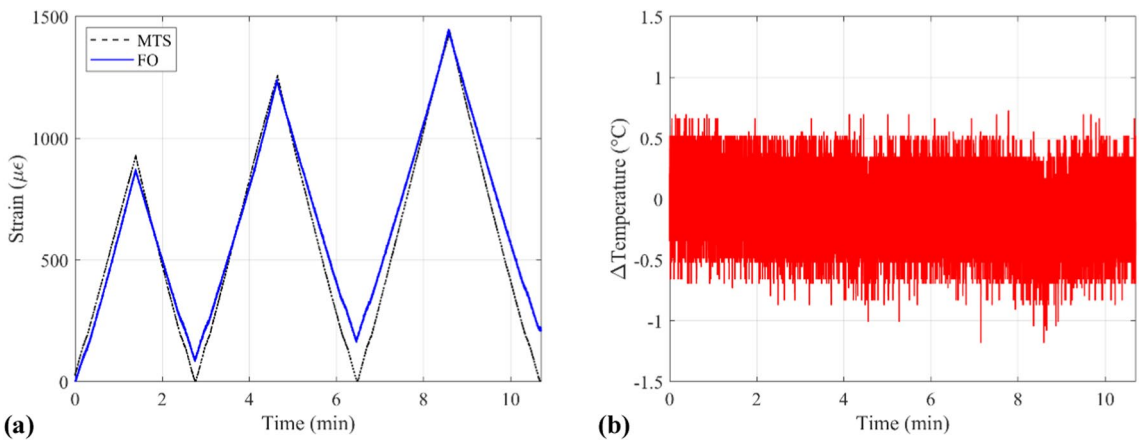

Figure 24 Strain **a** and temperature **b** trends as recalculated after decoupling signals from the four-point bending test on the sample equipped with the CT.

negligible, risking compromising the adhesion of the sensor. However, an accurate design can easily fix this issue.

In conclusion, the study demonstrates the feasibility of using thermal spray as an alternative for fixing and protecting FOs on metallic structures. As for the FOs, this method provides an excellent adhesion at the interface between the metallic coating and the fiber, the preservation of the structural integrity of the fiber itself and a precise measurement of strain acquired, thanks to the low temperature of process and excellent quality of the metallic coating. Also advantageous is the quality of the adhesion of the coating itself (virtually no defects even in the presence of the FOs) and the deposition efficiency obtained with the thermal spray process.

Acknowledgements

Authors gratefully thank Ing. Stefano Procopio and Fioravante Corasaniti from Thermospray S.r.l. (www.thermospray.it) for the production of the samples and the technical advice on the technique.

Author contributions

All authors contributed, to a different extent based on their skills and levels of experience, to the design and plan of the research, to the execution of experiments and data collection, to the analysis of the results and to the writing of the manuscript.

Funding

Open access funding provided by Politecnico di Milano within the CRUI-CARE Agreement.

Declarations

Conflicts of interest Authors have no conflicts of interest to disclose.

Data availability The data that support the findings of this study are available from the corresponding author upon request.

Ethical approval Not applicable.

References

[1] Betz DC, Staudigel L, Trutzel MN, Kehlenbach M (2003) Structural monitoring using fiber-optic bragg grating sensors. Struct Health Monit 2:145–152

[2] Wu T, Liu G, Fu S, Xing F (2020) Recent progress of fiber-optic sensors for the structural health monitoring of civil infrastructure. Sensors 20(16):4517–4543

[3] Wu Z, Zhang J, Tang Y (2012) Multiple purposes of long-gauge fiber optic sensors towards structural health monitoring. In: Proceedings of the 12th International Symposium on Structural Engineering, ISSE. p 163

[4] Alwis LS, Bremer K, Roth B (2021) Fiber optic sensors embedded in textile-reinforced concrete for smart structural health monitoring: a review. Sensors 21(15):4948–4972

[5] Bremer K, Wollweber M, Weigand F, Rahlves M, Kuhne M, Helbig R, Roth B (2016) Fibre optic sensors for the structural health monitoring of building structures. Procedia Technol 26:524–529

[6] Tsuda H, Lee JR, Guan Y, Takatsubo J (2007) Investigation of fatigue crack in stainless steel using a mobile fiber bragg grating ultrasonic sensor. Opt Fiber Technol 13:209–214

[7] Bettini P, Di Landro L, Airoldi A, Baldi A, Sala G (2011) Characterization of the interface between composites and embedded fiber optic sensors or NiTiNOL wires. Procedia Eng 10:3490–3496

[8] Grandal T, Fraga S, Vazquez JA, Zornoza A (2016) Technique for embedding fiber optics in metallic structures for smart material applications. In: 8th European workshop on structural health monitoring, EWSHM, Vol 3

[9] Müller MS, Hoffmann L, Lautenschlager T, Koch AW (2008) Soldering fiber bragg grating sensors for strain

measurement. In: 19th international conference on optical fibre sensors, Vol 7004
[10] Kim SI, Jung HY, Yang S, Yoon J, Lee H, Ryu W (2022) 3D printing of a miniature turbine blade model with an embedded fibre bragg grating sensor for high-temperature monitoring. Virtual Phys Prototyp 17(2):156–169
[11] Zou R, Liang X, Chen Q, Wang M, Zaghloul MA, Lan H, Buric MP, Ohodnicki PR, Chorpening B, To AC, Chen KP (2020) A digital twin approach to study additive manufacturing processing using embedded optical fiber sensors and numerical modeling. J Lightw Technol 38(22):6402–6411
[12] Grandal T, Zornoza A, Fraga S, Castro G, Sun T, Grattan KT (2018) Laser cladding-based metallic embedding technique for fiber optic sensors. J Lightwave Technol 36(4):1018–1025
[13] Havermann D, Mathew J, MacPherson WN, Hand DP, Maier RRJ (2015) Measuring residual stresses in metallic components manufactured with fibre bragg gratings embedded by selective laser melting. In: 24th international conference on optical fibre sensors, Vol 9634, p 96340
[14] Stoll P, Mathew J, Spierings A, Bauer T, Maier RRJ, Wegener K (2016) Embedding fibre optical sensors into SLM parts. In: Solid freeform fabrication 2016 proceedings of the 27th annual international solid freeform fabrication symposium—an additive manufacturing conference, SFF 2016. pp 1815–1825
[15] Mathew J, Havermann D, Polyzos D, MacPherson WN, Hand DP, Maier RRJ (2015) SS316 structure fabricated by selective laser melting and integrated with strain isolated optical fiber high temperature sensor. In: 24th international conference on optical fibre sensors, Vol 9634, p 96340Q
[16] Manns M, Raza SM, Morez D, Schreiber F, Engel B (2024) Embedding optical fiber with laser metal deposition. Prog Addit Manuf
[17] Petrie CM, Sridharan N, Hehr A, Norfolk M, Sheridan J (2019) High-temperature strain monitoring of stainless steel using fiber optics embedded in ultrasonically consolidated nickel layers. Smart Mater Struct 28(8):085041–085074
[18] Hyer HC, Sweeney DC, Petrie CM (2022) Functional fiber-optic sensors embedded in stainless steel components using ultrasonic additive manufacturing for distributed temperature and strain measurements. Addit Manuf 52:102681–102691
[19] Monaghan T, Capel AJ, Christie SD, Harris RA, Friel RJ (2015) Solid-state additive manufacturing for metallized optical fiber integration. Compos Part A: AppL Sci Manuf 76:181–193
[20] He XL, Wang ZQ, Wang DH, Wang XB, Liu Y, Jiang FC, Yuan LB (2019) Optical fiber sensor for strain monitoring of metallic device produced by very high-power ultrasonic additive manufacturing. IEEE Sens J 19(22):10680–10685
[21] He X, Ma C, Wang X, Wang Z, Jiang F, Yuan L (2020) Metallic structure functional sensor based on embedded PANDA fiber by ultrasonic additive manufacturing. Appl Optics 59(16):4880–4887
[22] Schomer JJ, Hehr AJ, Dapino MJ (2016) Characterization of embedded fiber optic strain sensors into metallic structures via ultrasonic additive manufacturing. In: Sensors and smart structures technologies for civil, mechanical, and aerospace systems 2016, Vol 9803. p 980320
[23] Chilelli SK, Schomer JJ, Dapino MJ (2019) Detection of crack initiation and growth using fiber bragg grating sensors embedded into metal structures through ultrasonic additive manufacturing. Sensors 19(22):4917–4936
[24] Hehr A, Norfolk M, Wenning J, Sheridan J, Leser P, Leser P, Newman JA (2018) Integrating fiber optic strain sensors into metal using ultrasonic additive manufacturing. Jom 70:315–320
[25] Hehr A, Norfolk M, Sheridan J, Davis M, Leser W, Leser P, Newman JA (2019) Spatial strain sensing using embedded fiber optics. JOM 71:1528–1534
[26] Zhang X, Hua Z, Picklesimer CA, Chuirazzi WC, Sun C, McMurtrey MD, Rufner J (2024) Integrating fiber optic sensors into metallic components for sensing in harsh environments. Opt Laser Technol 170:110188–110201
[27] Boulos MI, Fauchais PL, Heberlein JVR (2021) Thermal spray fundamentals. In: Thermal spray fundamentals
[28] Qadir D, Sharif R, Nasir R, Awad A, Mannan HA (2024) A review on coatings through thermal spraying. Chem Papers 78(1):71–91
[29] Kumar SS, Prasad CD, Hanumanthappa H (2024) Role of thermal spray coatings on erosion, corrosion, and oxidation in various applications: a review. J Bio-and Tribo-Corros 10(2):22–32
[30] Pakmehr M, Moslehi B, Costa J, Black RJ, Sotoudeh V, Behbahani A (2014) A review of fiber optic technology for turbine engine instrumentation channel: control, PHM, and test cell applications. In: 50th AIAA/ASME/SAE/ASEE joint propulsion conference 2014
[31] Ghelichi R, Guagliano M (2009) Coating by the cold spray process: a state of the art. Frattura Ed Integrità Strutturale 3:30–44
[32] Singh H, Sidhu TS, Kalsi SBS (2012) Cold spray technology: future of coating deposition processes. Frattura Ed Integrita Strutturale 22:69–84
[33] Li W, Yang K, Yin S, Yang X, Xu Y, Lupoi R (2018) Solid-state additive manufacturing and repairing by cold spraying: a review. J Mater Sci Technol 34:440–457

[34] Modi SC, Calla E (2001) A Study of High-Velocity Combustion Wire Molybdenum Coatings. J Therm Spray Technol 10:480–486

[35] Talib RJ, Saad S, Toff MR, Hashim H (2003) Thermal spray coating technology: a review. Solid State Sci Technol 11(1):109–117

[36] Sala G, Di Landro L, Airoldi A, Bettini P (2015) Fibre optics health monitoring for aeronautical applications. Meccanica 50:2547–2567